Supplementary Information

Continuous Control of Thermal Responses in Dynamic Crystals via Solid Solution Engineering

Jiantao Meng,[a] Yahui Su,[b] Hang Zhu,[a] Wenrui Chen,[a] An Chen,[b] Yuan Su,*[b] and Ting Cai*[ab]

[a] State Key Laboratory of Natural Medicines, Department of Pharmaceutics, School of Pharmacy, China Pharmaceutical University, Nanjing 211198, China

[b] Department of Pharmaceutical Engineering, School of Engineering, China Pharmaceutical University, Nanjing 211198, China

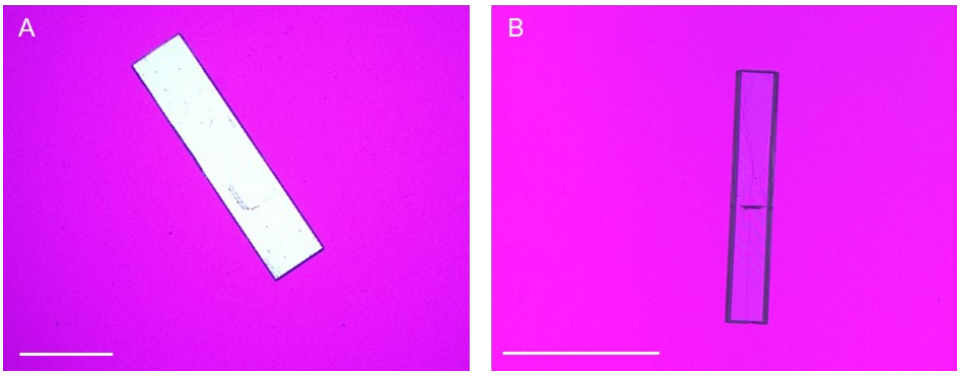

Figure S1. Single-crystal morphologies of PCV (A) and GCV (B). Scale bar = 200 μm.

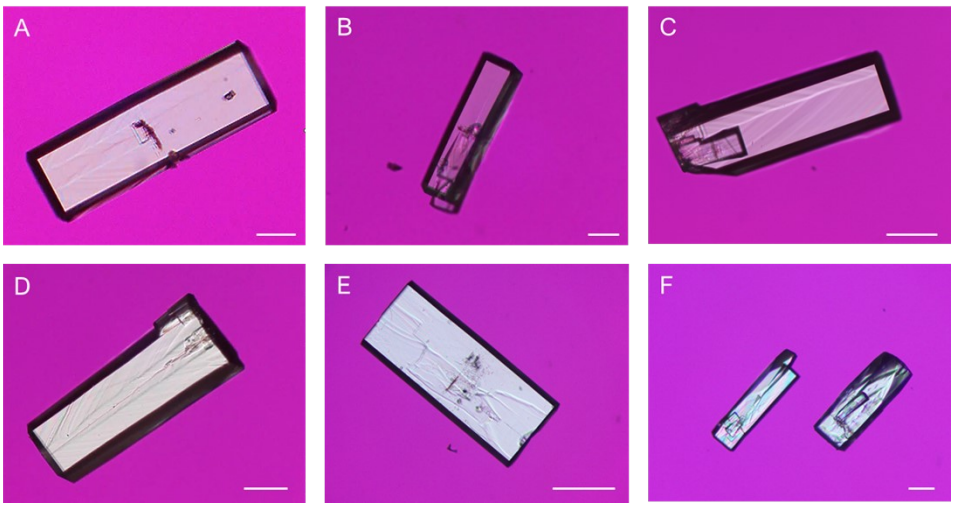

Figure S2. Single-crystal morphologies of solid solutions. Panels A-F correspond to $PCV_{0.90}$-$GCV_{0.10}$, $PCV_{0.80}$-$GCV_{0.20}$, $PCV_{0.75}$-$GCV_{0.25}$, $PCV_{0.70}$-$GCV_{0.30}$, $PCV_{0.50}$-$GCV_{0.50}$, and $PCV_{0.10}$-$GCV_{0.90}$, respectively. Scale bar = 100 μm.

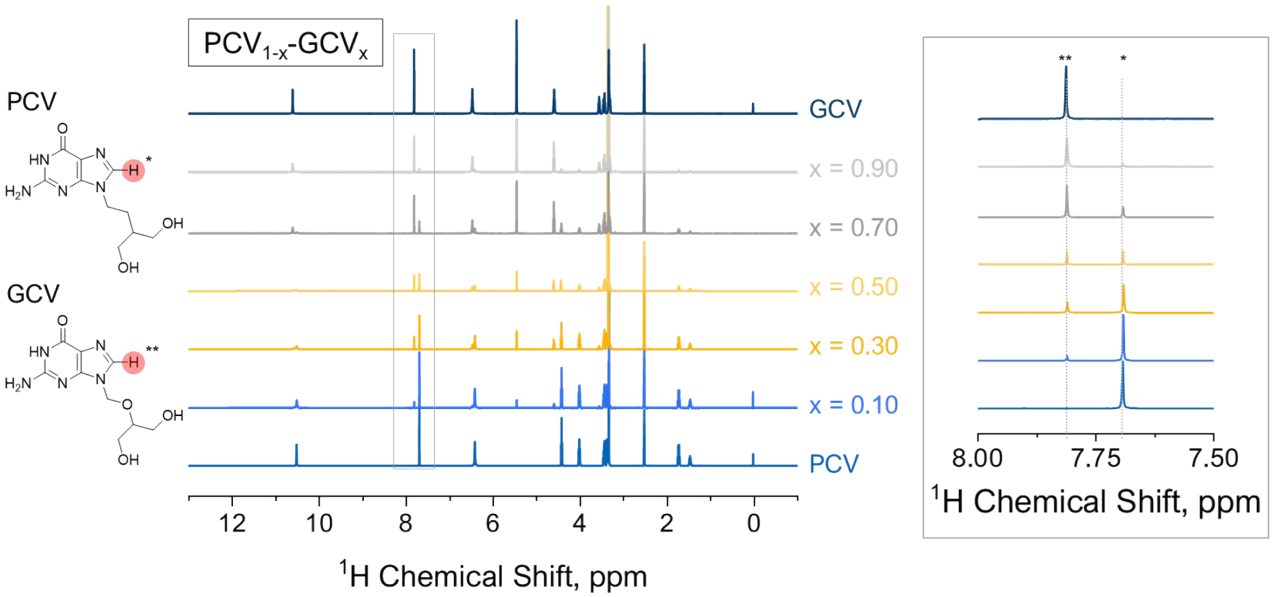

Figure S3. ^{1}H-NMR spectra of the solid-solution single crystals. The non-labile proton on the aromatic heterocycle (peak at ~7.75 ppm) was used to quantify the stoichiometric ratios of the solid solutions.

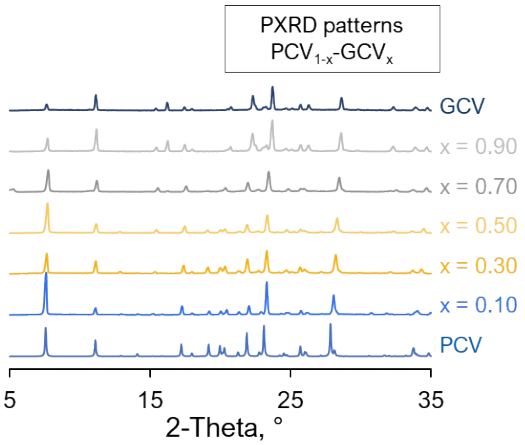

Figure S4. PXRD patterns of the solid solutions. The similarity of the diffraction profiles and the gradual shift in peak positions indicate that these crystals possess comparable structures, which progressively vary with composition.

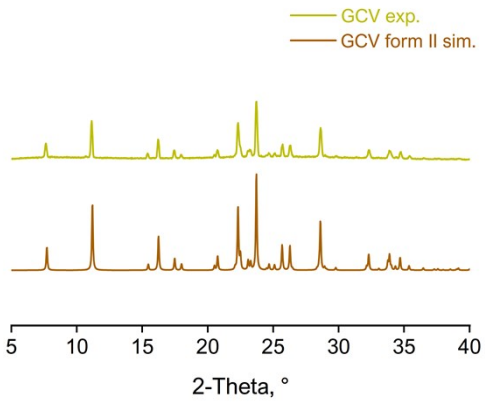

Figure S5. PXRD patterns of the GCV form II. The experimental results correspond well with the simulated results from the single crystal structure (CCDC: 714337).

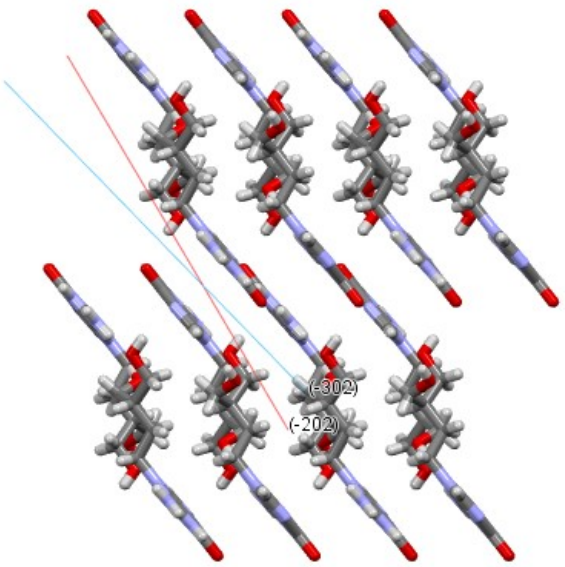

Figure S6. The layered structure of PCV is approximately parallel to the $(\bar{2}02)$ and $(\bar{3}02)$ planes.

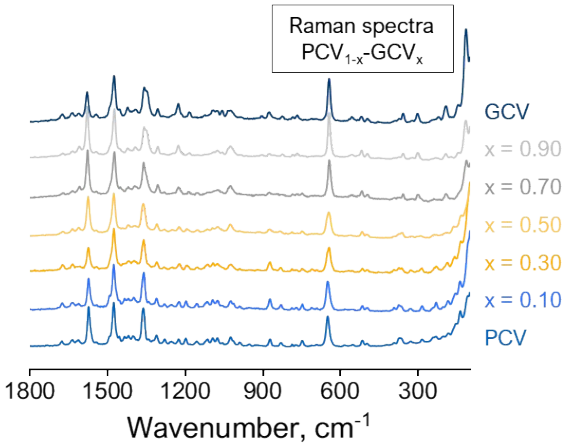

Figure S7. Raman spectra of the solid solutions. The comparable spectral profiles and gradual shifts in characteristic peaks suggest that the crystals share similar structures, while exhibiting progressive structural variations with changing composition.

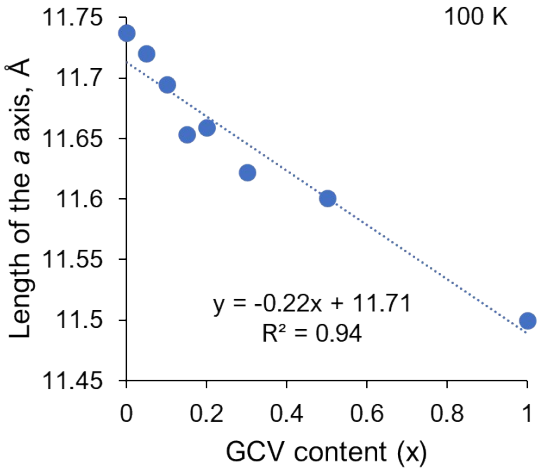

Figure S8. Variation of the *a*-axis parameter of PCV, the solid solutions, and GCV at 100 K as a function of composition.

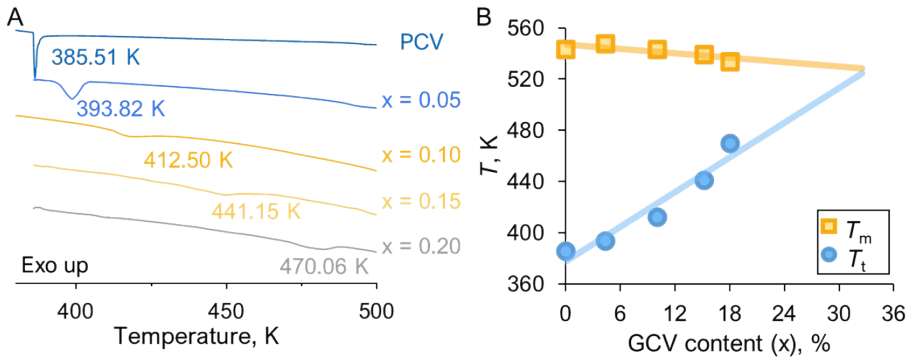

Figure S9. (A) DSC profile recorded by heating the solid solutions over the temperature of the phase transition. (B) The T_t and T_m as a function of GCV content. Solid solutions with GCV content over 30% don't exhibit phase transition behaviors.

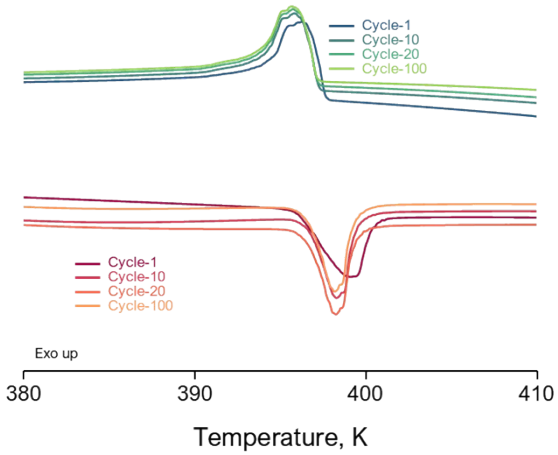

Figure S10. Phase transition signals of $PCV_{0.95}$-$GCV_{0.05}$ under different heating-cooling cycles recorded by DSC, demonstrating excellent thermal stability and fatigue resistance of the crystal.

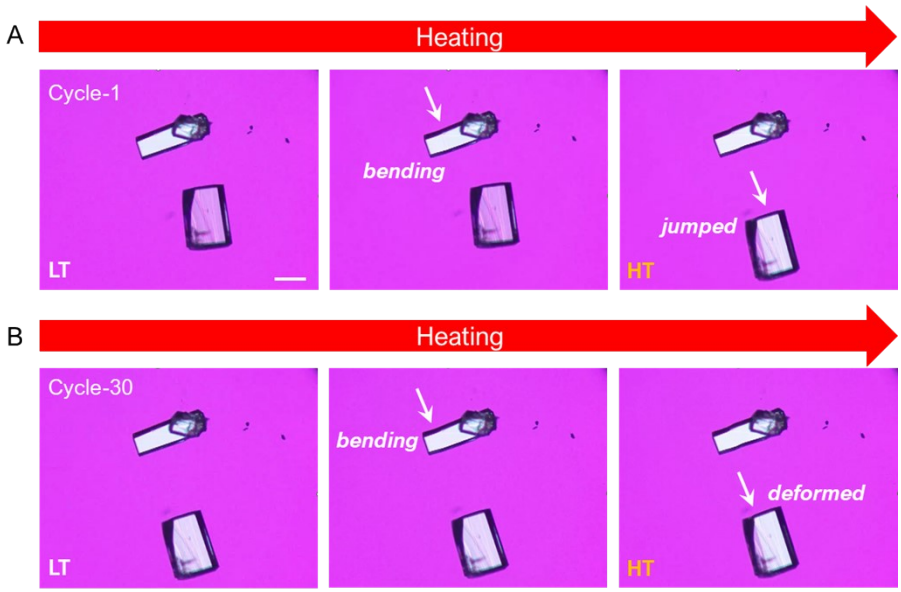

Figure S11. Phase transition behavior of $PCV_{0.95}$-$GCV_{0.05}$ observed by HS-PLM during the first and 30th heating-cooling cycles, illustrating the crystal's excellent fatigue resistance.

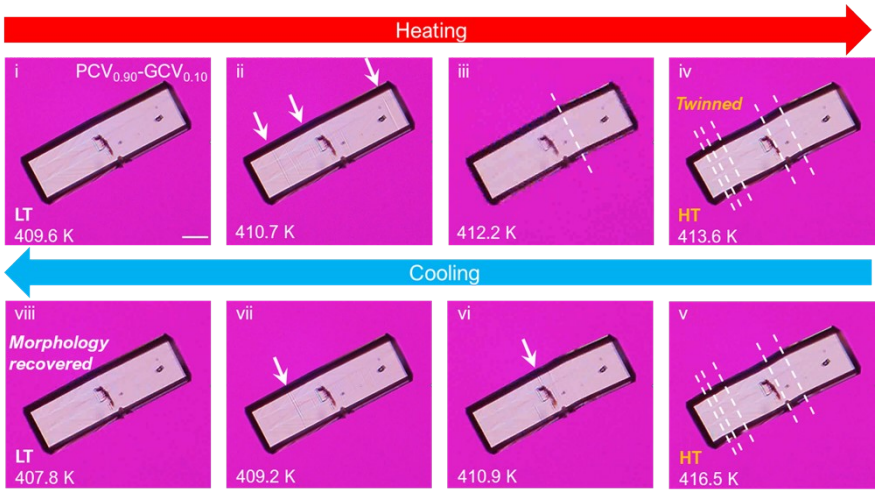

Figure S12. Reversible bending and morphology recovery of $PCV_{0.90}$-$GCV_{0.10}$ during the phase transition, resembling the behavior of PCV crystals. The arrows indicate the phase front, while the dashed lines mark the formation of twin boundaries. Scale bar = 100 μm.

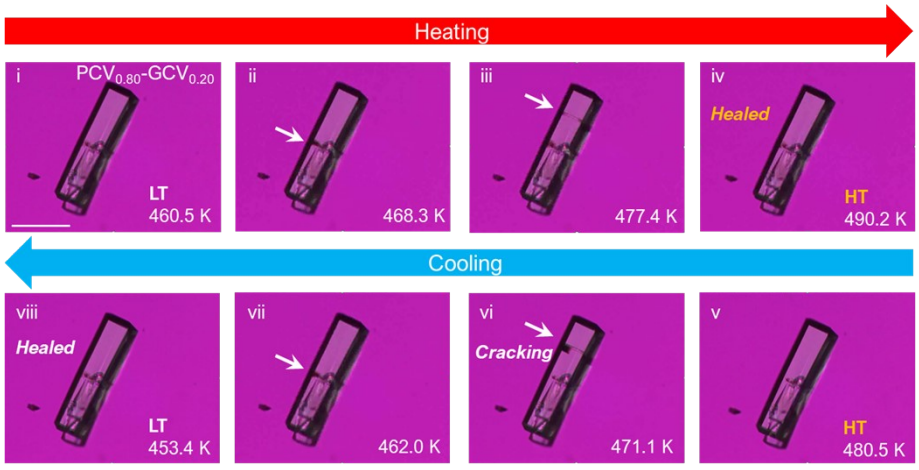

Figure S13. Cracking and self-healing behaviors of $PCV_{0.80}$-$GCV_{0.20}$ during the phase transition. The arrows indicate the formation of cracks. Scale bar = 100 μm.

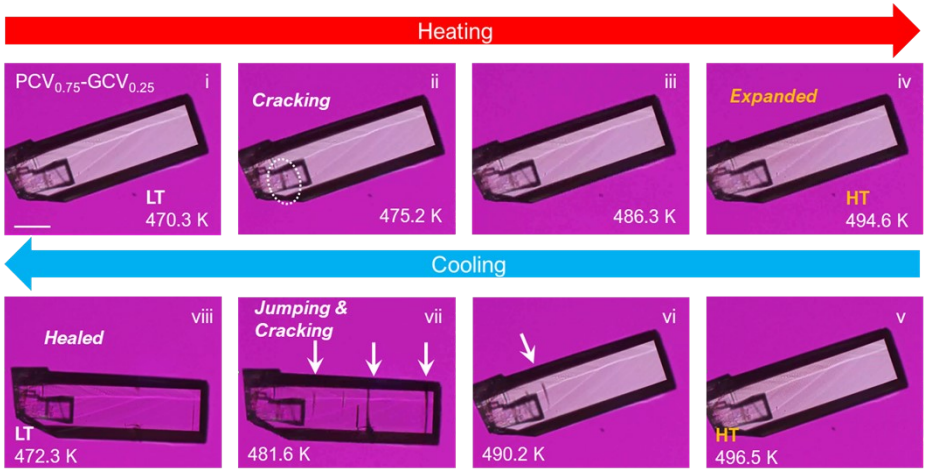

Figure S14. Cracking and self-healing behaviors of $PCV_{0.75}$-$GCV_{0.25}$ during the phase transition. The arrows indicate the formation of cracks. The crystal exhibited jumping during this process. Scale bar = 100 μm.

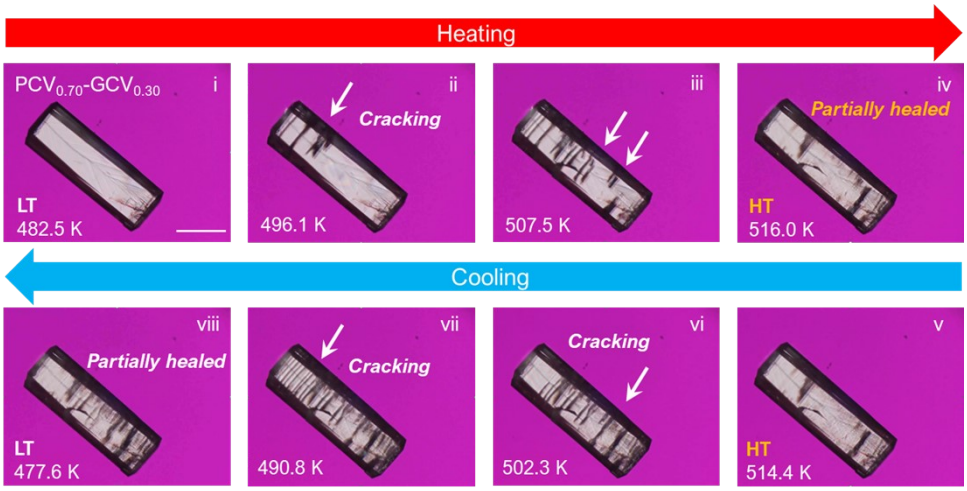

Figure S15. Cracking and self-healing behaviors of $PCV_{0.70}$-$GCV_{0.30}$ during the phase transition. The arrows indicate the formation of cracks. Due to the severe cracking and the T_t being close to the T_m, the crystal exhibited only partial self-healing. Scale bar = 100 μm.

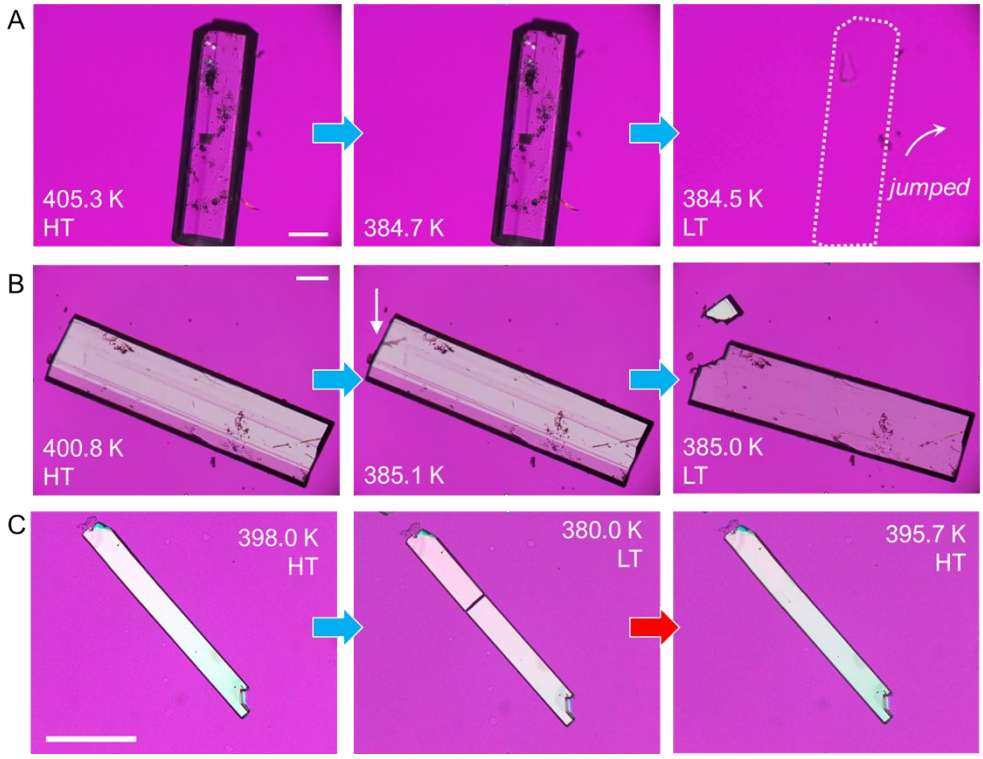

Figure S16. Thermosalient and self-healing effects of PCV crystals. (A) Jumping and (B) cracking observed during the thermosalient effect. (C) Cracking and self-healing observed during phase transition cycles. Scale bar = 100 μm.

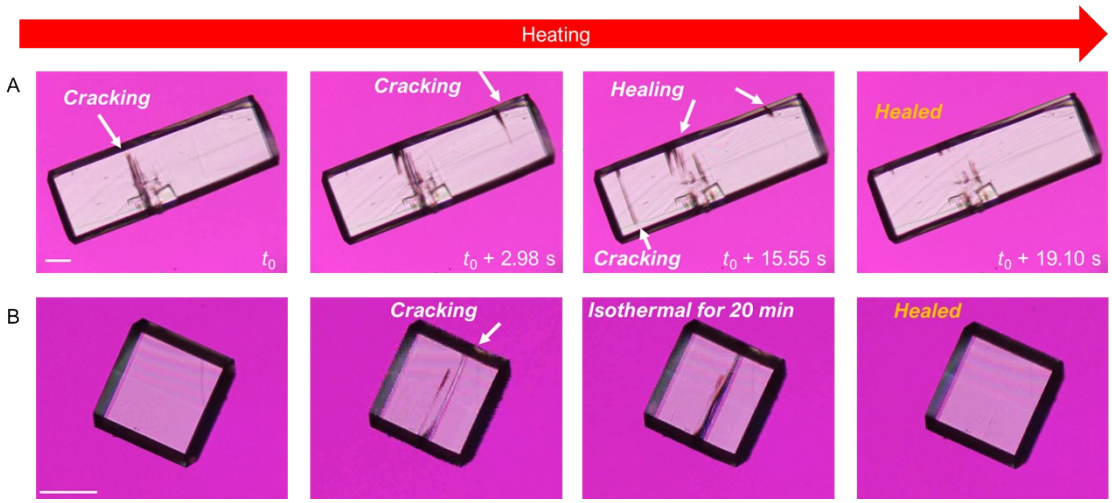

Figure S17. Cracking and self-healing behavior of $PCV_{0.85}$-$GCV_{0.15}$ during heating. (A) Cracking and slow healing of the crystal at a heating rate of 20 K min^{-1}; the healing time for an individual crack is typically longer than 15 s. (B) Cracks can remain dynamically stable for at least 20 min during the phase transition under isothermal conditions. Scale bar = 100 μm.

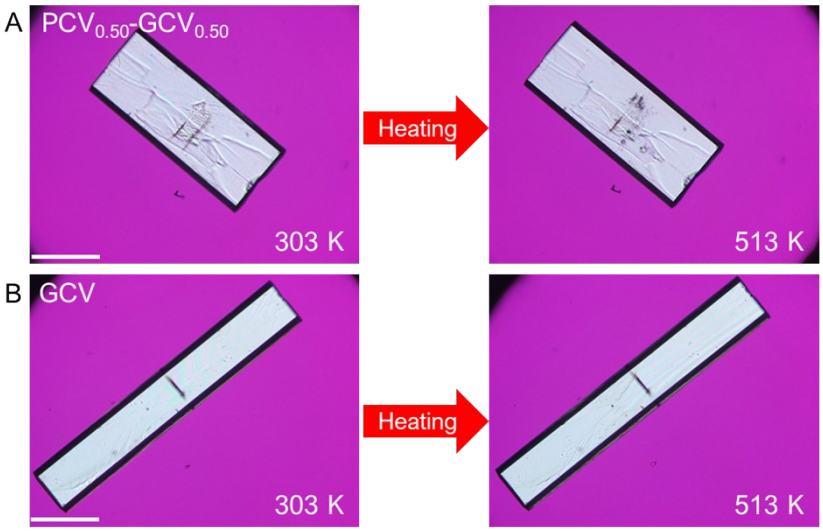

Figure S18. $PCV_{0.50}$-$GCV_{0.50}$ and GCV crystals did not exhibit any mechanical responses over the temperature range from room temperature to near their T_m. Scale bar = 100 μm.

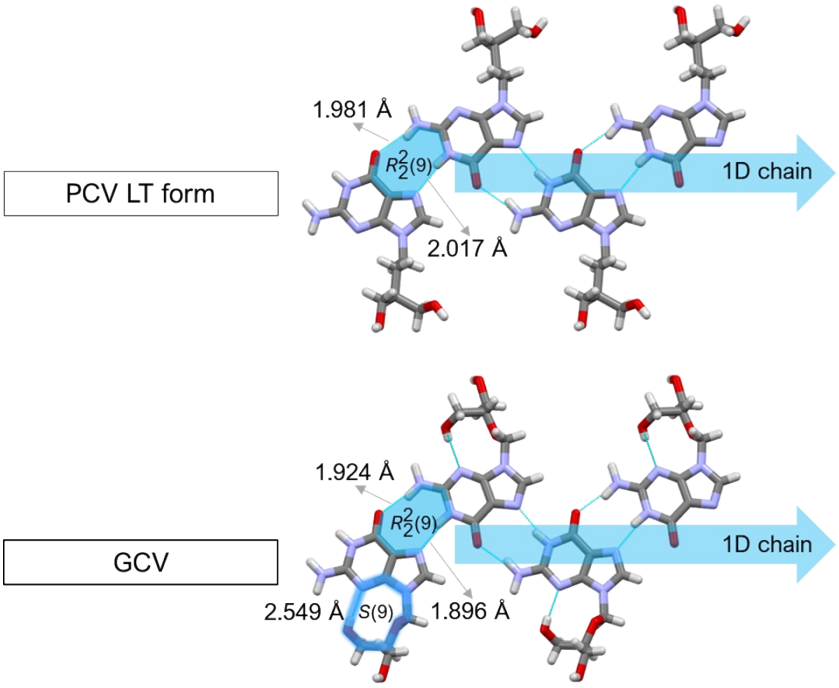

Figure S19. Structural motifs of the PCV LT form and GCV. In both crystals, the molecules form one-dimensional (1D) chain structures along the *b*-axis through dimerization ($R_2^2(9)$).

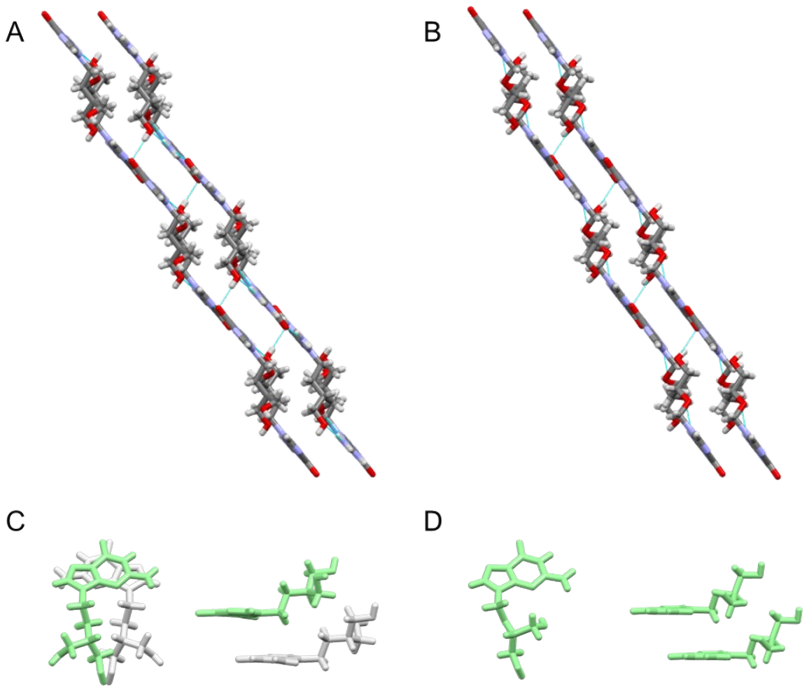

Figure S20. (A-B) Schematic representation of the layered packing and interlayer hydrogen bonds in PCV (left) and GCV (right). (C-D) π…π stacking arrangements in PCV (left) and GCV (right). Due to the different space groups, the two crystals exhibit distinct aromatic stacking patterns.

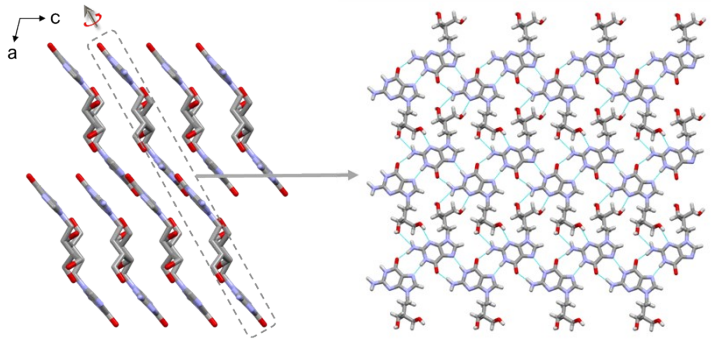

Figure S21. Layered packing and intralayer structures of the $PCV_{0.90}$-$GCV_{0.10}$ LT form. This crystal exhibit nearly identical structures to PCV crystal.

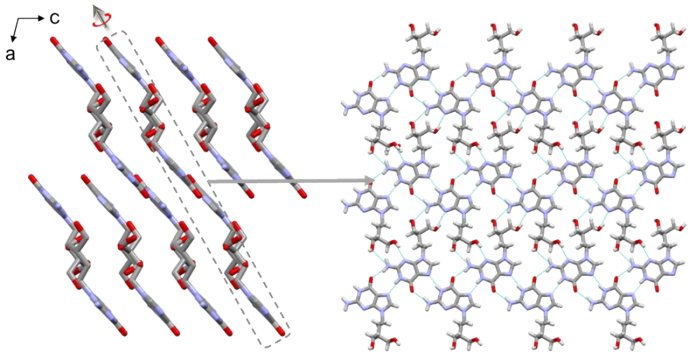

Figure S22. Layered packing and intralayer structures of the $PCV_{0.70}$-$GCV_{0.30}$ LT form. This crystal exhibit nearly identical structures to PCV crystal.

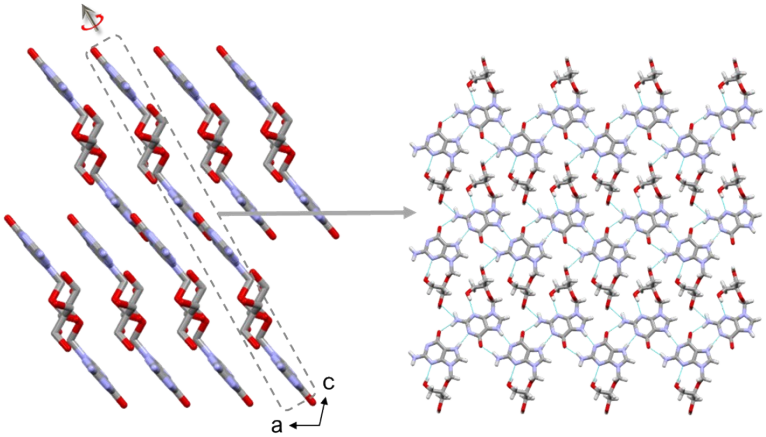

Figure S23. Layered packing and intralayer structures of the $PCV_{0.50}$-$GCV_{0.50}$. This crystal exhibit nearly identical structures to GCV crystal.

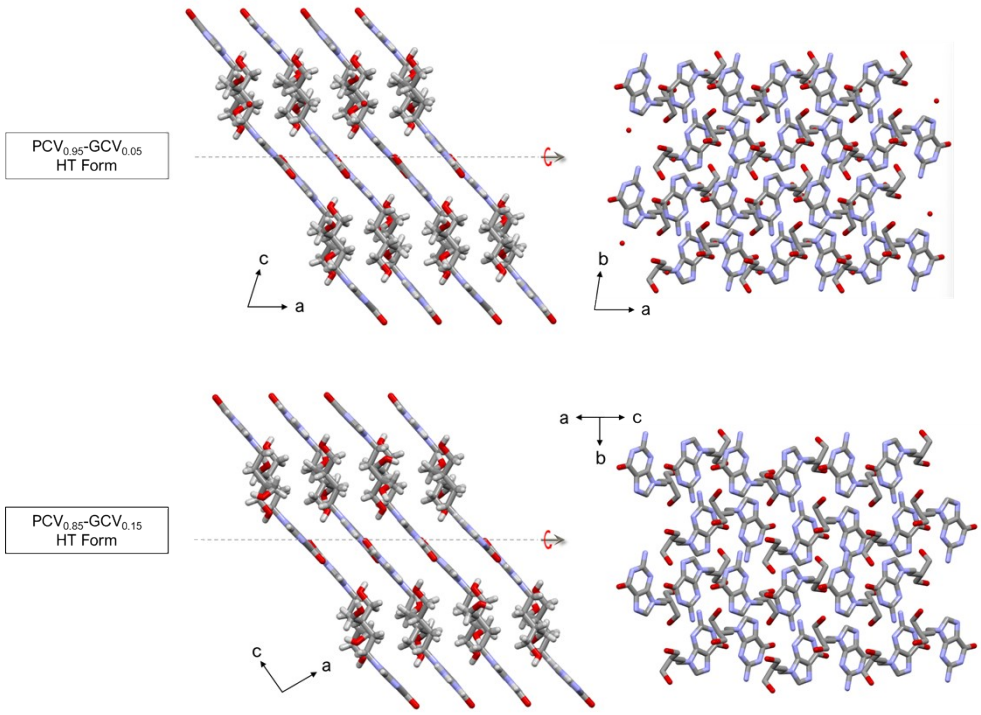

Figure S24. Packing patterns of the HT forms of $PCV_{0.95}$-$GCV_{0.05}$ and $PCV_{0.85}$-$GCV_{0.15}$. The two crystals differ in space group and lattice parameters: $PCV_{0.95}$-$GCV_{0.05}$ crystallizes in a triclinic system with α and γ angles deviating from 90°, whereas $PCV_{0.85}$-$GCV_{0.15}$ retains an orthogonal *b*-axis.

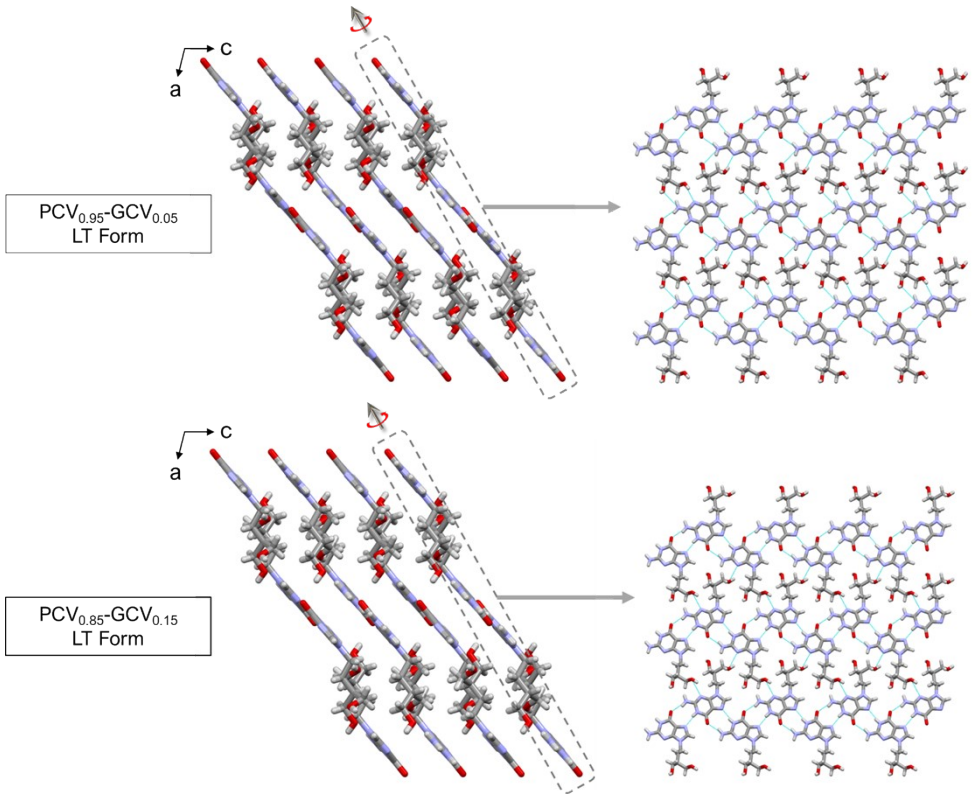

Figure S25. Layered packing of the $PCV_{0.95}$-$GCV_{0.05}$ and $PCV_{0.85}$-$GCV_{0.15}$ LT form. This crystal exhibit nearly identical structures to PCV crystal.

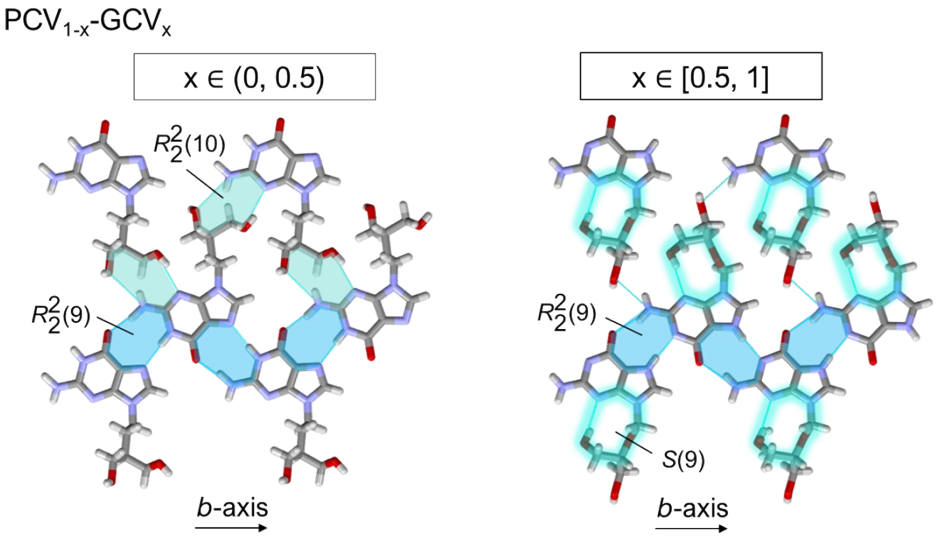

Figure S26. Structural motifs of solid solutions. In all crystals, the molecules form one-dimensional (1D) chain structures along the *b*-axis through dimerization ($R_2^2(9)$).

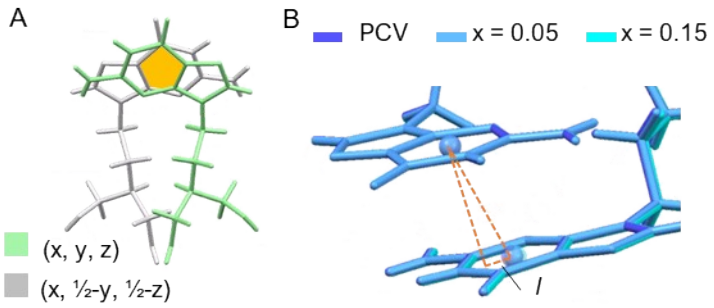

GCV content, x	*l*, Å
0	0.6987
0.05	0.6681
0.15	0.6262

Figure S27. (A) π…π stacking arrangement in the PCV crystal and solid solutions; the gray and green molecules represent two PCV molecules with different orientations. (B) Overlay views of the molecular packing of PCV, $PCV_{0.95}$-$GCV_{0.05}$ and $PCV_{0.85}$-$GCV_{0.15}$, highlighting the centroid-centroid distances. (C) The horizontal component of the centroid-centroid distance. The data points of $PCV_{0.90}$-$GCV_{0.10}$ and $PCV_{0.70}$-$GCV_{0.30}$ were not presented here due to the different test temperature.

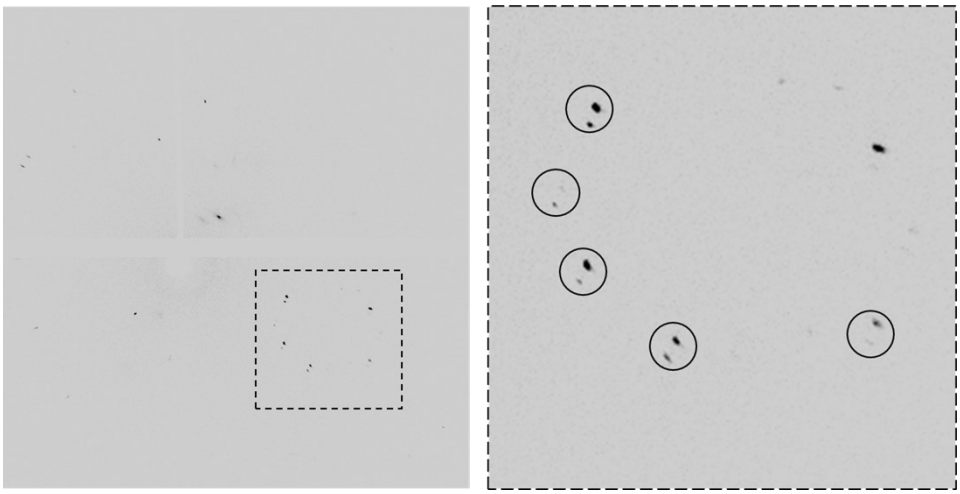

Figure S28. Two-dimensional diffraction patterns of a twinned $PCV_{0.95}$-$GCV_{0.05}$ crystal at 420 K.

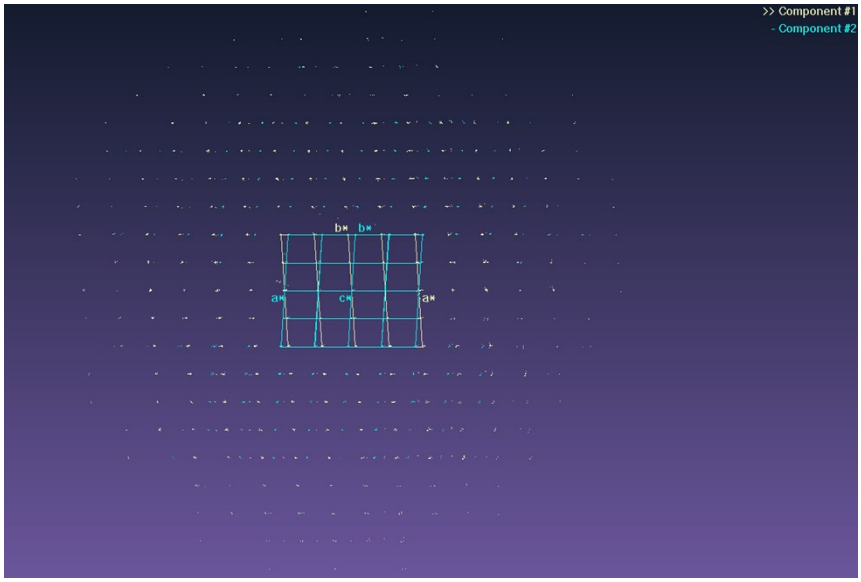

Figure S29. Ewald's diffraction sphere of a twinned $PCV_{0.95}$-$GCV_{0.05}$ crystal at 420 K.

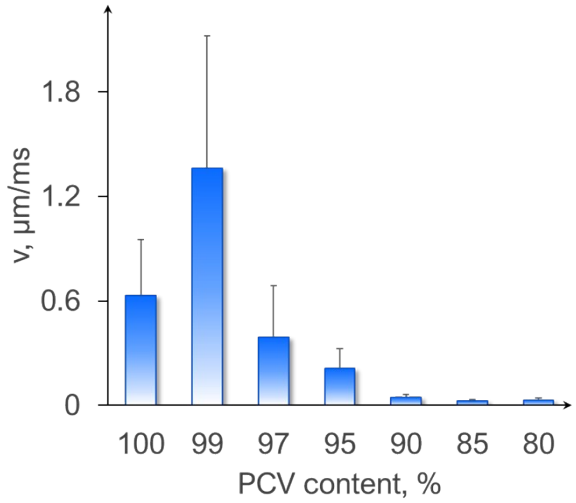

Figure S30. Variation of phase transition rate with composition.

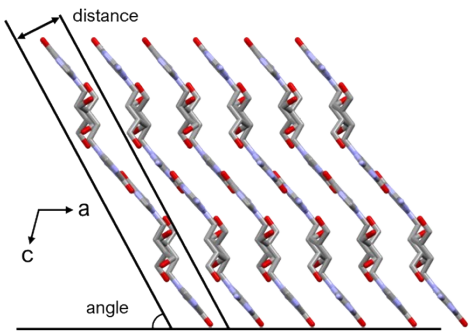

		LT	HT	variation
PCV	Angle, °	59.42	58.34	-1.82%
	Distance, Å	3.847	3.862	+0.39%
$PCV_{0.95}$-$GCV_{0.05}$	Angle, °	59.39	58.25	-1.92%
	Distance, Å	3.843	3.868	+0.65%
$PCV_{0.85}$-$GCV_{0.15}$	Angle, °	59.17	57.57	-2.70%
	Distance, Å	3.846	3.901	+1.43%

Figure S31. Interlayer distance and the angle (between the (100) to $(10\bar{1})$) of the $PCV_{0.95}$-$GCV_{0.05}$ and $PCV_{0.85}$-

$GCV_{0.15}$ two forms.

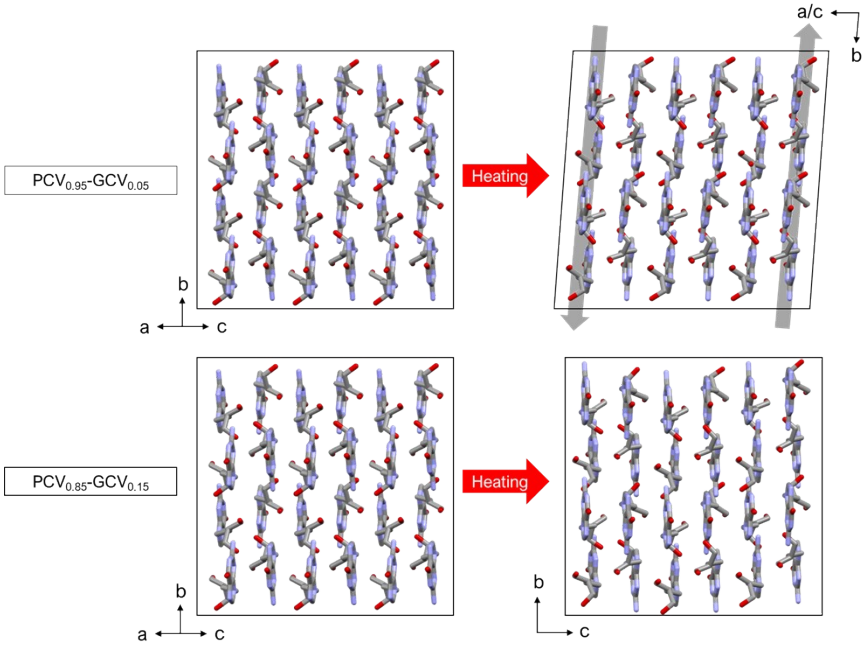

Figure S32. Layered structures of $PCV_{0.95}$-$GCV_{0.05}$ and $PCV_{0.85}$-$GCV_{0.15}$ observed perpendicular to the *b*-axis. The analysis reveals that the molecular layers of $PCV_{0.95}$-$GCV_{0.05}$ undergo relative slippage along the *b*-axis (follow the gray arrows) during the phase transition.

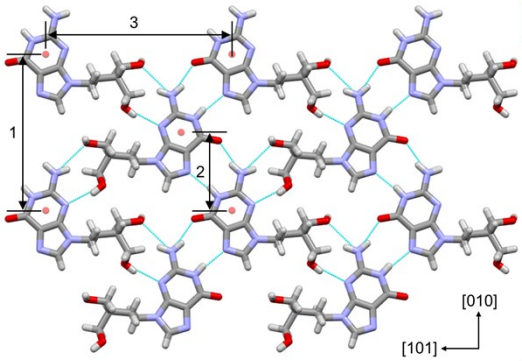

		LT	HT	variation
PCV	L1	10.88 Å	10.89 Å	0.09%
	L2	5.44 Å	4.23 Å	-22.20%
	L3	11.67 Å	11.64 Å	-0.26%
$PCV_{0.95}$-$GCV_{0.05}$	L1	10.89 Å	10.95 Å	0.52%
	L2	5.45 Å	5.54 Å	-0.14%
	L3	11.55 Å	11.63 Å	0.70%
$PCV_{0.85}$-$GCV_{0.15}$	L1	10.92 Å	11.06 Å	1.31%
	L2	5.45 Å	5.52 Å	1.37%
	L3	11.62 Å	11.48 Å	-1.20%

Figure S33. Layered structures of $PCV_{0.95}$-$GCV_{0.05}$ and $PCV_{0.85}$-$GCV_{0.15}$ observed perpendicular to the *b*-axis.

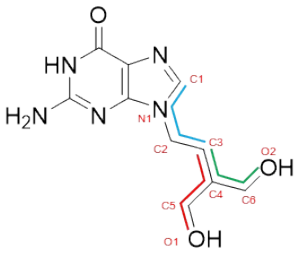

Torsion angle	C1-N1-C2-C3, °	C3-C4-C5-O1, °	C3-C4-C6-O2, °
$PCV_{0.95}$-$GCV_{0.05}$ 380 K	100.14	179.36	72.26
$PCV_{0.95}$-$GCV_{0.05}$ 420 K Z1	97.76	179.48	73.27
$PCV_{0.95}$-$GCV_{0.05}$ 420 K Z2	100.50	177.02	70.10
$PCV_{0.85}$-$GCV_{0.15}$ 400 K	99.73	179.89	72.10
$PCV_{0.85}$-$GCV_{0.15}$ 490 K Z1	100.71	177.28	72.03
$PCV_{0.85}$-$GCV_{0.15}$ 490 K Z2	98.13	178.07	69.87
$PCV_{0.85}$-$GCV_{0.15}$ 490 K Z3	98.88	175.55	79.55

Figure S34. Molecular structure of PCV, featuring a rigid aromatic ring and a flexible side chain. Atom labels and colored lines are drawn to determine torsion angles and analyze conformational changes during the phase

transition.

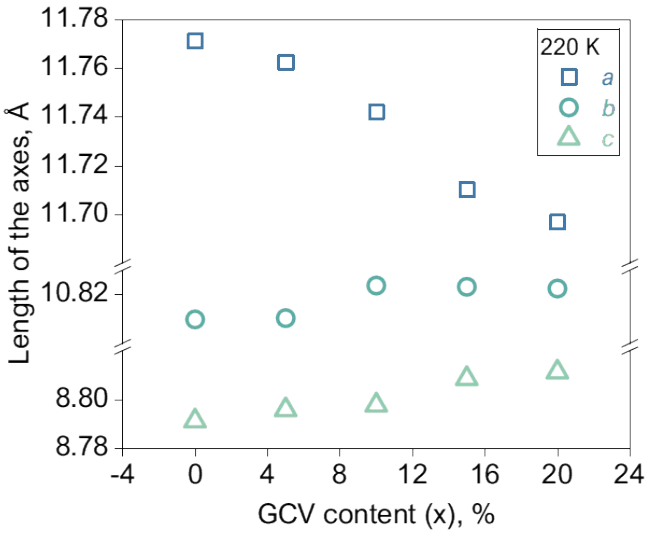

Figure S35. Summary of the unit cell parameters of PCV crystal and the solid solutions at 220 K. The plots show the temperature-dependent changes of the *a*, *b*, and *c* axes.

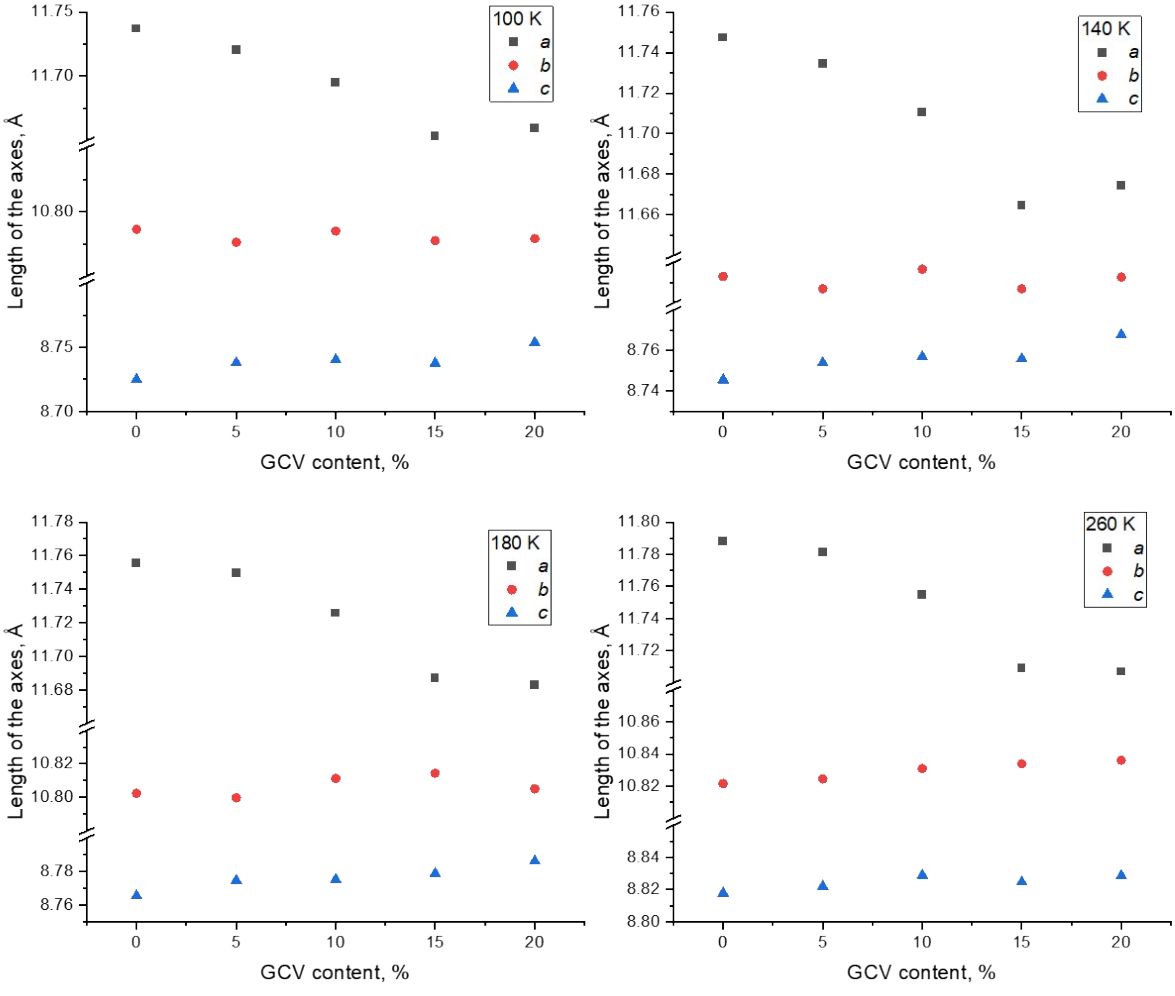

Figure S36. Summary of the unit cell parameters of PCV crystal and the solid solutions at different

temperatures. The plots show the temperature-dependent changes of the *a*, *b*, and *c* axes.

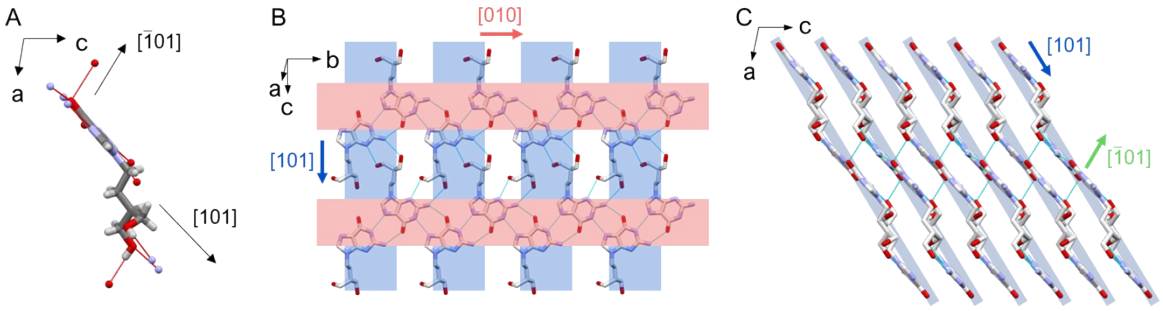

Figure S37. Intermolecular hydrogen-bonding motifs in PCV crystal and the solid solutions. Intermolecular hydrogen bond in a molecular (A), motif (B), and packing views (mainly in crystallographic directions of [010], [101], and [$10\bar{1}$]).

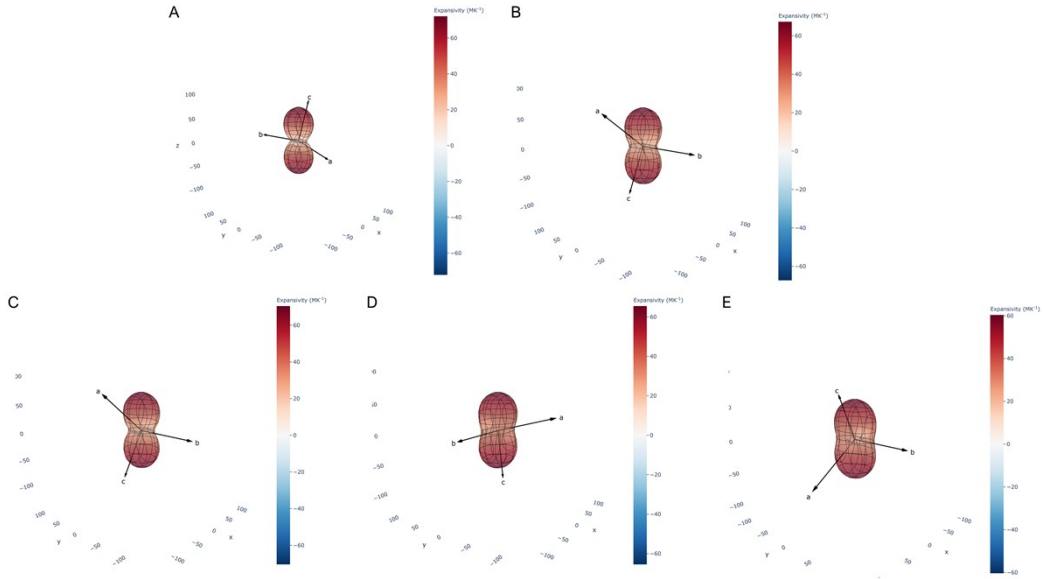

Figure S38. Expansivity indicatrix of PCV, $PCV_{0.95}$-$GCV_{0.05}$, $PCV_{0.90}$-$GCV_{0.10}$, $PCV_{0.85}$-$GCV_{0.15}$, and $PCV_{0.80}$-$GCV_{0.20}$, calculated using PasCal program.[1] A similar and gradually changing indicatrix indicates that the crystal structure and thermal expansion behavior undergo a systematic variation.

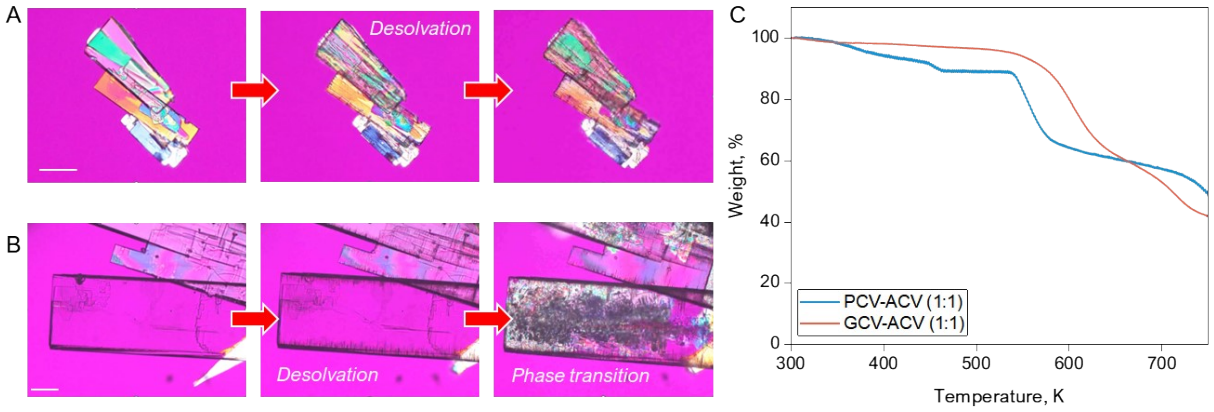

Figure S39. Screening and characterization of PCV-ACV and GCV-ACV solid solutions. (A) Desolvation and phase transition behavior of the PCV-ACV solid solution upon heating; (B) desolvation and phase transition behavior of the GCV-ACV solid solution upon heating; (C) TGA curves of PCV-ACV and GCV-ACV, indicating that both are solvates.

Table S1. Unit cell parameters of PCV, solid solutions, and GCV at 100 K across the composition range.

GCV content, %	*a*, Å	*b*, Å	*c*, Å	*α*, °	*β*, °	*γ*, °	*V*, Å^3
0	11.7371	10.7863	8.7252	90	99.281	90	1090.144
5	11.7206	10.7763	8.7378	90	99.264	90	1089.23
10	11.6948	10.785	8.7403	90	99.185	90	1088.26
15	11.6533	10.7775	8.7377	90	99.186	90	1083.34
20	11.6593	10.779	8.7538	90	99.138	90	1086.18
30	11.6218	10.7919	8.7804	90	99.008	90	1087.67
50	11.6008	10.7903	8.7106	90	98.684	90	1077.86
100	11.4997	10.7687	8.6424	90	98.691	90	1057.96

Table S2. Phase transition enthalpies ($\Delta^{HT}_{LT}H_m$) of PCV crystal and solid solutions. The values decrease significantly with increasing GCV content, and for the $PCV_{0.85}$-$GCV_{0.15}$ and $PCV_{0.80}$-$GCV_{0.20}$ samples, accurate measurement was no longer possible.

	PCV	$PCV_{0.95}$-$GCV_{0.05}$	$PCV_{0.90}$-$GCV_{0.10}$	$PCV_{0.85}$-$GCV_{0.15}$	$PCV_{0.80}$-$GCV_{0.20}$
$\Delta^{HT}_{LT}H_m$, KJ/mol	1.03	0.77	0.21	< 0.1	< 0.1

Table S3. Crystallographic data of the $PCV_{0.90}$-$GCV_{0.10}$, $PCV_{0.70}$-$GCV_{0.30}$, and $PCV_{0.50}$-$GCV_{0.50}$.

	PCV	$PCV_{0.90}$-$GCV_{0.10}$	$PCV_{0.70}$-$GCV_{0.30}$	$PCV_{0.50}$-$GCV_{0.50}$	GCV Form II
Empirical formula	$C_{10}H_{15}N_5O_3$	$C_{10}H_{15}N_5O_3$	$C_{9.7}H_{14.4}N_5O_{3.3}$	$C_9H_{13}N_5O_4$	$C_9H_{13}N_5O_4$
CCDC number	2313630	2520173	2520172	2520168	714337[2]
Formula weight	253	253.27	253.86	255.24	255.24
Temperature/K	380	100	100	100	293.1
Crystal system	monoclinic	monoclinic	monoclinic	monoclinic	monoclinic
Space group	$P2_1/c$	$P2_1/c$	$P2_1/c$	$P2_1$	$P2_1$
a/Å	11.8542(16)	11.7031(5)	11.6218(8)	4.3553(3)	4.3803(15)
b/Å	10.8829(13)	10.7835(4)	10.7919(7)	10.7903(7)	10.909(4)
c/Å	8.9354(12)	8.7394(4)	8.7804(6)	11.6008(9)	11.601(4)

α/°	90	90	90	90	90
β/°	99.888(5)	99.188(2)	99.008(3)	98.684(2)	99.11(3)
γ/°	90	90	90	90	90
V/Å^3	1135.6(3)	1088.76(8)	1087.67(13)	538.93(7)	547.4(3)
Z	4	4	4	2	2
ρ_{calc}g cm^{-3}	1.481	1.545	1.550	1.573	1.549
F(000)	536.0	536.0	536.0	268.0	268.0

Table S4. Crystallographic data of the $PCV_{0.95}$-$GCV_{0.05}$ and $PCV_{0.85}$-$GCV_{0.15}$ polymorphs.

	$PCV_{0.95}$-$GCV_{0.05}$		$PCV_{0.85}$-$GCV_{0.15}$	
	LT form	HT form	LT form	HT form
Empirical formula	$C_{10}H_{15}N_5O_3$	$C_{9.95}H_{14.9}N_5O_{3.05}$	$C_{10}H_{15}N_5O_3$	$C_{10}H_{16}N_5O_3$,2($C_{10}H_{15}N_5O_3$)
CCDC number	2520171	2520174	2520169	2520170
Formula weight	253.27	253.37	253.27	760.82
Temperature/K	380	420	400	490
Crystal system	monoclinic	Triclinic	monoclinic	monoclinic
Space group	$P2_1/c$	$P\bar{1}$	$P2_1/c$	$P2_1/n$
a/Å	11.8369 (3)	9.117 (4)	11.7938 (3)	13.6410 (5)
b/Å	10.8946 (3)	10.951 (5)	10.9225 (3)	11.0691 (4)
c/Å	8.9309 (2)	11.800 (4)	8.9572 (3)	23.4349 (9)
α/°	90	87.02 (3)	90	90
β/°	99.883 (1)	80.55 (2)	99.877 (2)	93.007 (2)
γ/°	90	86.23 (4)	90	90
V/Å^3	1134.62 (5)	1158.6 (8)	1136.75 (6)	3533.7 (2)
ρ_{calc}g cm^{-3}	1.483	1.453	1.480	1.430
Z	4	4	4	4
F(000)	536.0	536.0	536.0	1612.0

Table S5. Unit cell parameters of a twinned $PCV_{0.95}$-$GCV_{0.05}$ crystal at 420 K.

	a, Å	b, Å	c, Å	α, °	β, °	γ, °	V, Å^3	Ratio, %

Domain-1	9.0715	10.8953	11.7790	87.239	80.461	86.134	1144.7	77.7%
Domain-2	9.0735	10.8942	11.7736	87.337	80.508	86.301	1144.7	21.5%

Table S6. Summary of VT unit cell parameters for PCV crystal and solid solutions.

	T, K	*a*, Å	*b*, Å	*c*, Å	*α*, °	*β*, °	*γ*, °	*V*, Å^3
PCV	100	11.7371	10.7863	8.7252	90	99.2810	90	1090.144
	140	11.7474	10.7931	8.7456	90	99.3817	90	1094.034
	180	11.7557	10.8024	8.7656	90	99.4966	90	1097.886
	220	11.7712	10.8098	8.7911	90	99.5718	90	1103.035
	260	11.7883	10.8216	8.8178	90	99.6793	90	1108.854
$PCV_{0.95}$-$GCV_{0.05}$	100	11.7206	10.7763	8.7378	90	99.264	90	1089.23
	140	11.7343	10.7871	8.754	90	99.333	90	1093.41
	180	11.7496	10.7998	8.7746	90	99.427	90	1098.4
	220	11.7625	10.8103	8.7957	90	99.528	90	1103
	260	11.7813	10.8246	8.822	90	99.625	90	1109.21
$PCV_{0.90}$-$GCV_{0.10}$	100	11.6948	10.785	8.7403	90	99.185	90	1088.26
	140	11.7105	10.7967	8.7571	90	99.252	90	1092.8
	180	11.7257	10.8113	8.7752	90	99.389	90	1097.53
	220	11.7421	10.8237	8.7976	90	99.487	90	1102.82
	260	11.755	10.831	8.829	90	99.566	90	1108.463
$PCV_{0.85}$-$GCV_{0.15}$	100	11.6533	10.7775	8.7377	90	99.186	90	1083.34
	140	11.6648	10.7870	8.7561	90	99.200	90	1087.59
	180	11.6871	10.8145	8.7788	90	99.231	90	1095.20
	220	11.7001	10.8214	8.7990	90	99.347	90	1099.26
	260	11.7093	10.8340	8.8248	90	99.449	90	1104.34
$PCV_{0.80}$-$GCV_{0.20}$	100	11.6593	10.779	8.7538	90	99.138	90	1086.18
	140	11.6743	10.7927	8.7679	90	99.206	90	1090.5
	180	11.6828	10.8052	8.7862	90	99.307	90	1094.52
	220	11.6968	10.8225	8.8112	90	99.427	90	1100.3
	260	11.707	10.8361	8.8288	90	99.425	90	1104.8

Table S7. Principal axes of thermal expansion and corresponding coefficients for PCV crystal and solid solutions, calculated using PasCal program.

				Direction		
	Axes	α (MK^{-1})	$\sigma\alpha$ (MK^{-1})	*a*	*b*	*c*
PCV	X_1	13.33	1.81	0.81	0	0.586
	X_2	20.2	0.953	0	1	0
	X_3	72.17	1.855	-0.293	0	0.956
	V	106.5	4.721			
$PCV_{0.95}$-$GCV_{0.05}$	X_1	17.8	0.849	0.771	0	0.636
	X_2	27.73	0.637	0	1	0
	X_3	67.3	2.578	-0.352	0	0.936
	V	113.7	4.056			
$PCV_{0.90}$-$GCV_{0.10}$	X_1	16.92	1.03	0.715	0	0.699
	X_2	27.52	1.274	0	1	0
	X_3	70.44	2.898	-0.435	0	0.9
	V	115.8	2.588			
$PCV_{0.85}$-$GCV_{0.15}$	X_1	34.1	1.62	0	1	0
	X_2	23.11	2.518	0.935	0	0.355
	X_3	65.45	2.276	-0.098	0	0.995
	V	123.8	2.838			
$PCV_{0.80}$-$GCV_{0.20}$	X_1	14.23	1.557	0.765	0	0.644
	X_2	33.31	0.401	0	1	0
	X_3	60.36	1.866	-0.367	0	0.93
	V	108.8	1.882			

References

1. Lertkiattrakul, M.; Evans, M. L.; Cliffe, M. J., PASCal Python: A Principal Axis Strain Calculator. *Journal of Open Source Software* **2023,** *8* (90), 5556.
2. Kawamura, T.; Hirayama, N., Crystal Structure of Ganciclovir. *X-ray Structure Analysis Online* **2009,** *25*, 51-52.